International Journal of Biological Macromolecules 325 (2025) 147296

Contents lists available at ScienceDirect

International Journal of Biological Macromolecules

journal homepage: www.elsevier.com/locate/ijbiomac

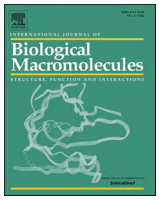

Single-step bleaching versus organosolv-bleaching of sugarcane bagasse: tuning TEMPO-oxidized nanocellulose morphology via delignification strategy

Eupidio Scopel [a,1], Lidiane O. Pinto [a], Camila A. Rezende [a,*]

[a] Universidade Estadual de Campinas - UNICAMP, Instituto de Química, 13083-970 Campinas, SP, Brazil

ARTICLE INFO

Keywords:
Cellulose nanofibril
Cellulose nanocrystal
Lignocellulosic biomass
Sugarcane bagasse
Bleaching

ABSTRACT

TEMPO-mediated oxidation is an effective and widely used method for producing carboxylated cellulose nanofibrils (CNFs) from lignocellulosic substrates. However, the morphology of the resulting nanocelluloses can vary significantly when TEMPO oxidation is applied to sugarcane bagasse (SCB) substrates with minimal lignin content, depending on the amount of oxidizing agent used. This work elucidates strategies for tailoring nanocellulose morphology from SCB by TEMPO oxidation and reveals the effect of a delignification step prior to bleaching on nanocellulose properties. To this end, two delignified substrates with minimum lignin content, obtained via sequential organosolv-bleaching or single-step bleaching, were subjected to TEMPO oxidation and ultrasonication. Although both substrates exhibited similar lignin contents, the use of a pre-delignification step was crucial for producing short particles characterized as cellulose nanocrystals (CNCs), whereas single-step bleaching produced CNFs. These findings highlight that morphological changes induced by the two-step delignification process, rather than lignin content alone, play a key role in determining the final nanocellulose morphology. Therefore, the most appropriate nanocellulose production route can be selected based on the target application, whether CNFs or CNCs are preferred.

1. Introduction

Nanocelluloses, also referred to as cellulose nanomaterials or cellulose nanoparticles, are a class of renewable materials primarily derived from lignocellulosic biomass [1,2]. Wood remains the predominant source of nanocelluloses since it is traditionally used in pulp and paper mills [3]. However, non-wood lignocellulosic biomasses, especially agro-industrial wastes, have attracted increasing attention due to their abundance, low cost, and origin as byproducts of crop processing [4].

Currently, agro-industrial residues are mainly landfilled or incinerated for energy recovery [4,5], despite their potential as substrates for producing bioproducts, including chemicals, fuels, and materials [4,6]. In this context, nanocellulose production from agro-industrial wastes offers a strategic route and opportunity for enhance biomass valorization due to their broad application potential, including the preparation of hydrogels [7], electronic devices [8], nanocomposites [9], aerogels and cryogels [10], films [11], and emulsions [12]. These applications leverage the unique properties of nanocelluloses, such as high aspect ratio, tunable surface chemistry, rheological behavior, and optical and barrier properties [13,14].

Nanocelluloses are generally classified into two main types: cellulose nanofibrils (CNFs) and cellulose nanocrystals (CNCs). Both CNFs and CNCs exhibit nanoscale cross-sections (2–20 nm) but differ in length and flexibility, resulting in different properties. CNFs are elongated and flexible structures, often several micrometers long, capable of forming gels at low concentrations (~1 wt%) due to their strong entanglement capacity [15]. In contrast, CNCs are short, rigid, and highly crystalline particles that exhibit chiral nematic ordering at higher concentrations [16], and provide excellent reinforcement to polymeric matrices in nanocomposites [17]. Given their structural and functional differences, distinct biomass processing routes are required to obtain CNFs or CNCs, depending on the intended application.

Regardless of whether CNFs or CNCs are the target, their production from lignocellulosic biomass typically begins with lignin removal, commonly referred to as delignification, to obtain a cellulose-enriched solid. This step is essential because lignocellulosic biomass consists

* Corresponding author.
E-mail addresses: eupidio.scopel@ubc.ca (E. Scopel), l136551@dac.unicamp.br (L.O. Pinto), camilaiq@unicamp.br (C.A. Rezende).
[1] Department of Wood Science, University of British Columbia, Vancouver, BC, V6T 1Z4, Canada (current address).

https://doi.org/10.1016/j.ijbiomac.2025.147296
Received 7 May 2025; Received in revised form 25 August 2025; Accepted 31 August 2025
Available online 1 September 2025

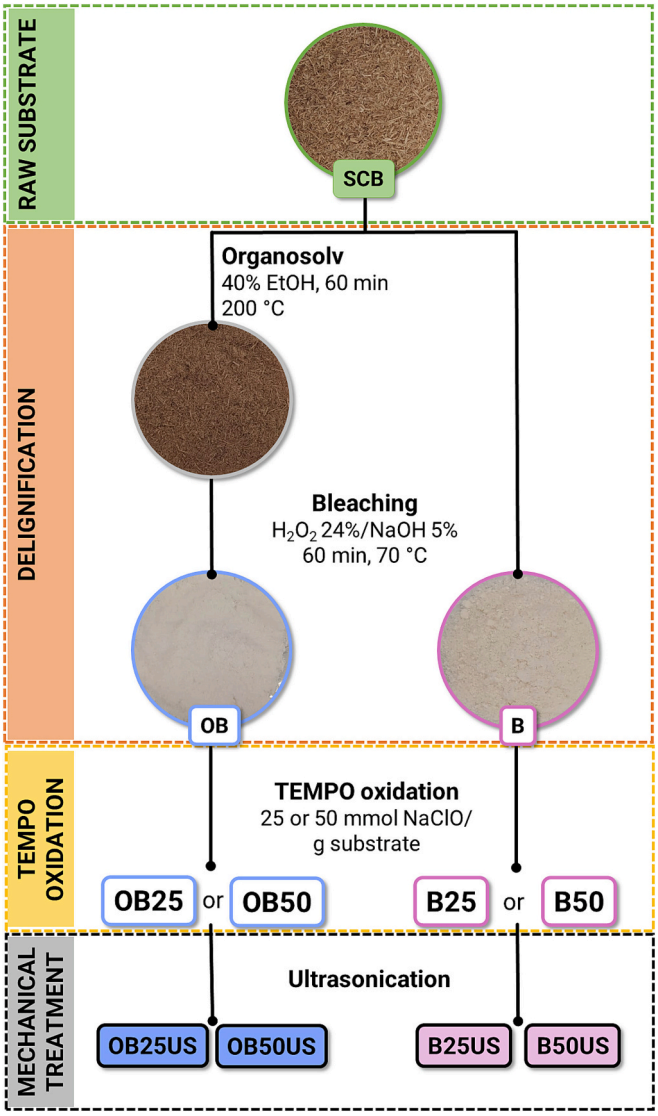

Fig. 1. Schematic representation of the nanocellulose production from SCB, comprising delignification (via sequential organosolv-bleaching or single-step bleaching), TEMPO-mediated oxidation using 25 or 50 mmol NaClO per gram of substrate, and mechanical treatment by ultrasonication.

mainly of cellulose, hemicellulose, and lignin, which are linked through chemical bonds and intermolecular interactions that form a natural composite structure [14,18]. Therefore, lignin acts as a barrier to the subsequent chemical, biological, or mechanical treatments required to isolate nanocelluloses [19]. Following delignification, CNFs are typically obtained by mechanically fibrillating the cellulose-rich substrate using microfluidizers, homogenizers, or ultrasonicators [20]. Prior to mechanical treatment, the cellulose-rich material can be chemically [21,22] or enzymatically [23,24] treated to lower energy consumption and improve fibrillation efficiency. Conversely, CNCs are predominantly produced via acid hydrolysis [25], which removes amorphous cellulose domains and releases crystalline regions as colloidal particles [26]. The resulting CNCs typically carry surface functional groups such as sulfate half-esters, which are most prevalent due to the use of sulfuric acid in hydrolysis [27]. However, the surface chemistry can vary depending on the production route [28].

Oxidation catalyzed by 2,2,6,6-tetramethylpiperidine-1-oxyl (TEMPO) is a well-established method for modifying cellulose pulps to produce carboxylated CNFs. In TEMPO-mediated oxidation, the primary hydroxy groups of cellulose are converted into carboxyl groups under mild conditions, which enhances electrostatic repulsion and facilitates CNF isolation [14]. Although less common, CNCs can also be produced via TEMPO oxidation under specific conditions [29–31], typically requiring higher concentrations of oxidizing agent. Notably, CNC production via TEMPO oxidation is acid-free and conducted under milder conditions compared to conventional acid hydrolysis [31].

Sugarcane bagasse (SCB) has emerged as a promising substrate for nanocellulose production since it is highly available as a byproduct of sucrose and ethanol mills in countries like Brazil [4,32]. Previous studies have shown that CNCs can be obtained from SCB subjected to organosolv treatment followed by a two-step bleaching process as the delignification method, and subsequent TEMPO oxidation using NaClO concentrations higher than 25 mmol/g substrate [30]. In that study, CNC production was attributed to the increased surface charge resulting from the higher concentration of oxidizing agents. A similar rationale was proposed for CNC formation from TEMPO-oxidized microcrystalline cellulose and bleached softwood substrates [31].

Since variations in oxidizing agent concentration may influence nanocellulose production, previous studies have focused on the TEMPO oxidation step [30,31]. Investigating the impact of delignification strategies is however essential to identify the factors that drive CNC rather than CNF formation from SCB. Such understanding should also enable the development of more effective nanocellulose production routes, including biomass fractionation strategies.

This study aimed to identify the key factors governing the formation of CNFs or CNCs from SCB and to propose strategies for tuning nanocellulose morphology by altering the delignification route. Two substrates with similarly low lignin contents, which were obtained via either sequential organosolv-bleaching or single-step bleaching, were subjected to TEMPO oxidation at two levels of oxidizing agent to assess the influence of delignification strategy. The results indicate that single-step bleaching produces CNFs with reduced fiber damage, while sequential organosolv-bleaching enables acid-free production of carboxylated CNCs. This work thus provides a direct comparison between delignification strategies under identical oxidation conditions, isolating the effect of pretreatment on the final nanocellulose morphology.

2. Experimental

2.1. Materials

Sugarcane bagasse was kindly provided by Raízen® (Piracicaba, Brazil), dried in a convection oven (Tecnal, TE-394/3) at 60 °C for 8 h, milled using a knife mill (Arthur H. Thomas Co – Standard model 3) to a particle size below 2 mm, and stored in plastic containers. NaOH (P.A.), H_2O_2 (29 % concentration), NaBr (P.A.), and ethanol (99.5 % concentration) were purchased from Synth® (Diadema, Brazil); TEMPO was obtained from Sigma Aldrich® (St. Louis, MO, USA); and NaClO (10–12 % purity) was supplied from Êxodo Científica® (Sumaré, Brazil). All reagents were used as received.

2.2. Nanocellulose production

An overview of the nanocellulose production routes is provided in Fig. 1. In the first approach, raw SCB underwent sequential delignification consisting of organosolv extraction followed by bleaching (sample denoted as "OB"). In the second approach, bleaching was applied directly to raw SCB (sample denoted as "B"). After delignification, both substrates were subjected to TEMPO oxidation and subsequent mechanical treatment to produce nanocelluloses. Detailed descriptions of each process are provided in the subsequent sections.

2.2.1. Delignification

Organosolv treatments were performed using a 40 % (*v*/v) ethanol-water mixture at 200 °C for 1 h, with a solvent-to-biomass ratio of 10

Table 1
Chemical composition of raw, organosolv-bleached (OB), and directly bleached (B) SCB substrates.

Sample	Composition (wt%)				Total (%)	Remaining mass from 100 g of raw SCB
	Cellulose	Hemicellulose	Lignin	Ashes		
Raw SCB	39 ± 1	29 ± 2	33 ± 1	2 ± 1	103 ± 3	100
OB[a]	80 ± 2	13.2 ± 0.2	5.0 ± 0.2	0.9 ± 0.1	99 ± 2	24 ± 3
B	74 ± 3	16.8 ± 0.3	3.4 ± 0.2	3.7 ± 0.1	98 ± 3	45 ± 4

[a] OB substrate was obtained from bleaching organosolv-treated materials, which initially contained 71 ± 2 % cellulose, 11.2 ± 0.1 % hemicellulose, 14.8 ± 0.2 % lignin, and 1.5 ± 0.1 % ash. After the organosolv step, the solid yield was 42 ± 4 g per 100 g of raw SCB.

mL/g. Afterward, the reaction mixture was cooled to room temperature in an ice bath for 1 h. The solid was then separated using a nylon sieve (75 μm pore size), rinsed with ethanol to prevent lignin reprecipitation onto the cellulose fibers, and thoroughly washed with tap water until the rinsing water became colorless.

Bleaching was applied to both organosolv-treated and raw substrates [33], yielding the OB and B samples, respectively. Briefly, 10 g of dried biomass were dispersed in 200 mL of 5 wt% NaOH solution in a 2000 mL Erlenmeyer flask. Then, 200 mL of 24 % (*v*/v) H_2O_2 were added dropwise under continuous magnetic stirring (450 rpm) to minimize foam formation. The mixture was subsequently stirred at 70 ± 5 °C for 1 h. After that, it was cooled to room temperature on the bench (40 min), and the solid was recovered using a nylon sieve (75 μm pore size). The solid was washed with tap water until neutral pH was reached, dried at 60 °C in a convection oven for 6 h, and stored in plastic bags for subsequent chemical and morphological characterizations, as well as nanocellulose production.

2.2.2. TEMPO oxidation

TEMPO-mediated oxidation was conducted using the TEMPO/NaBr/NaClO system, following a previously established protocol [21]. Two NaClO concentrations (25 and 50 mmol/g substrate) were used, resulting in samples designated with the suffixes 25 and 50, respectively (Fig. 1). Briefly, 1 g of substrate (dry weight) was dispersed in 100 mL of deionized water 24 h before the reaction. Subsequently, 0.016 g of TEMPO and 0.1 g of NaBr were added and stirred until fully dissolved (~10 min). NaClO was then added, marking the beginning of the reaction. The initial pH was adjusted to 10 by the dropwise addition of 3 mol/L HCl. The reaction mixture was stirred at 350 rpm for 130 min. The pH was monitored every 10 min and maintained at 10.0 ± 0.2 adding 3 mol/L NaOH. After the reaction, the solids were washed by centrifugation (3500 rpm, 10 min, 8 cycles) and stored as 0.8 wt% dispersions in deionized water.

2.2.3. Mechanical treatment

Dispersions of oxidized pulp (0.8 wt%) were homogenized using an Ultra-Turrax disperser (IKA T25) at 7000 rpm for 5 min. Subsequently, ultrasonication was performed using a probe sonicator (Eco-Sonics QR550) at 60 % amplitude (330 W, 20 kHz) for 15 min in intermittent cycles (5 min on/5 min off) in an ice bath. The suffix "US" was added to the sample codes. As a proof of concept, selected samples B25 and OB25 were also mechanically treated in a microfluidizer (M110P, Microfluidics Corp.) equipped with *Z*-shaped interaction chambers (200 μm inner diameter). Based on previous reports, the samples were passed through the microfluidizer eight times [20]. The suffix "MF" was added to the sample names (B25MF and OB25MF).

2.3. Characterization

2.3.1. Chemical composition

The contents of cellulose, hemicellulose, lignin, extractives, and ashes in the raw, organosolv, and bleached substrates were determined according to the National Renewable Energy Laboratory protocol [34].

2.3.2. Atomic force microscopy (AFM)

Nanocelluloses were analyzed by AFM in non-contact mode under ambient conditions, using a Shimadzu SPM-9600 microscope equipped with silicon tips (NCHR Pointprobe, Nanoworld) featuring a cantilever spring constant of 42 N/m and nominal resonance frequency of 318 kHz. Prior to imaging, nanocellulose dispersions were diluted to 0.0025 wt%, drop-cast onto freshly cleaved mica substrates, and dried in a desiccator. The diameters and lengths of the nanocelluloses were measured using Gwyddion 2.56 software, with 150 individual particles analyzed per sample to generate diameter and length distribution histograms.

2.3.3. Field emission electron scanning microscopy (FESEM)

The morphology of the raw, delignified, and oxidized substrates was analyzed using FESEM (FEI Quanta 250) operated at 2 kV. Prior to imaging, dried samples were sputter-coated with iridium at 11.3 mV for 120 s using a Baltec coater (Oerlikon-Balzers). For oxidized samples, the dispersions were freeze-dried (Terroni, LS Series) prior to analysis. Each sample was examined in multiple regions and representative imagines were selected to characterize morphological features.

2.3.4. Degree of polymerization (DP)

The average DP of cellulose was determined by viscosimetry analysis in accordance ISO 5351 with minor modifications. Briefly, B, OB, B25, and OB25 samples were dried and subsequently dissolved in a copper ethylenediamine (CED) solution (0.5 mol/L). The intrinsic viscosity ([η]) was measured using a capillary viscometer at 25 °C, and the DP was calculated using the Mark-Houwink equation: DP = [η]/0.42 [35,36].

2.3.5. Conductometric titration

The carboxylate groups (-COO^-) present in the B25, B50, OB25, and OB50 samples were quantified by conductometric titration following previously reported procedures [37].

2.3.6. Zeta potential

The zeta potential of nanocellulose dispersions (0.05 wt%) at pH 5 was measured using a Zetasizer Nano ZS-Zen3600 (Malvern Instruments). Measurements were performed in triplicate, each run consisting of at least 10 scans acquired in backscattering mode (173°).

2.3.7. Rheology

Flow behavior of nanocellulose dispersions (1 wt%) was evaluated using a Haake MARS 60 rheometer (Thermo Fisher Scientific). Measurements were conducted at 25 °C using a double-gap geometry (DG41) for OB25US and a parallel plate geometry (35 mm, P35) for B25. Each sample was subjected to a pre-shear at 0.001 s^{-1} for 100 s, followed by a shear rate sweep from 0.001 to 1000 s^{-1}.

2.3.8. Thermogravimetric analysis (TGA)

TGA was performed using a TGA-DTA 6200 analyzer (Seiko Instruments) under a nitrogen atmosphere. Approximately 5 mg of each dry sample was heated from room temperature to 600 °C at a constant rate of 20 °C/min.

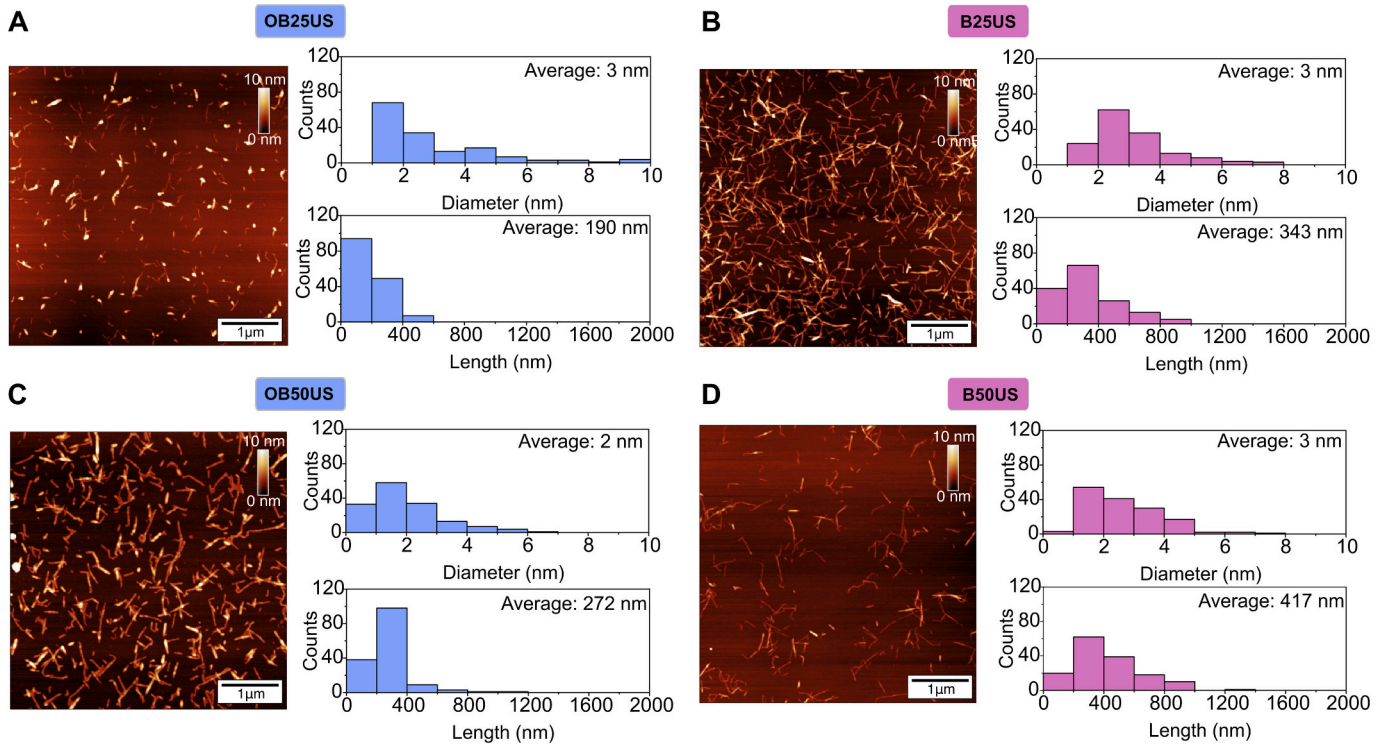

Fig. 2. Morphology of nanocelluloses and their respective diameter and length histograms of samples: A) OB25US; B) B25US; C) OB50US; D) B50US.

3. Results and discussion

3.1. Biomass chemical composition

Two distinct delignification strategies were evaluated to obtain cellulose-enriched substrates, as described in Fig. 1: (i) a sequential treatment comprising organosolv extraction followed by bleaching (referred to as OB), and (ii) a single-step bleaching (referred to as B). While the sequential delignification-bleaching route represents a more conventional approach, single-step bleaching is simpler, involving only one chemical stage, which may reduce fiber degradation and process costs.

In this study, single-step bleaching was explored with two main objectives: first, to assess whether a minimal residual lignin content is sufficient for CNC production from SCB or if multiple delignification stages are necessary, based on prior work using sequential organosolv and bleaching treatments [30]. Secondly, the single-step bleaching was applied to evaluate the feasibility of reducing the number of delignification steps in the nanocellulose production process from SCB.

The first goal was to obtain similar lignin contents in the substrates using distinct delignification strategies. Table 1 presents the chemical composition of the resulting solids. Both the sequential (OB) and single-step (B) delignification routes led to similarly reduced lignin contents (3.4–5 wt%), meeting the intended target. Cellulose content increased from 39 wt% in raw SCB to 74–80 wt% in the delignified samples, while hemicellulose content decreased from 29 wt% to 13–17 wt%. The lower hemicellulose content observed in OB may result from its additional removal during organosolv treatment, which was conducted at 200 °C. At this temperature, autohydrolysis makes the medium acidic, promoting hemicellulose hydrolysis and solubilization [38]. Given the comparable final compositions of OB and B, the organosolv step does not appear to be mandatory when the sole objective is lignin removal. This finding is relevant from a process optimization standpoint, as it simplifies the preparation of bleached SCB pulps. In addition, single-step bleaching enables fair comparisons between substrates obtained through distinct routes but chemically convergent routes.

On the other hand, the solid yield after delignification differed substantially between the two methods: 24 and 45 g from 100 g of raw SCB for OB and B, respectively. This difference can be attributed to the mass loss during organosolv extraction, which alone produced 42 g of solid from 100 g of raw SCB. When bleaching was applied to this pretreated material, the increased fiber accessibility likely enhanced further delignification, contributing to a lower final yield for OB.

Bleaching has previously demonstrated high efficacy in removing lignin from SCB substrates [30,33,39]. Its effectiveness stems from the synergistic action of the reactants: NaOH promotes lignin removal via hydrolysis of ester bonds in lignin-carbohydrate complexes, while H_2O_2 oxidizes carbonyl and quinoid structures in lignin side chains [40]. As a result, the bleached substrates appear white due to the chromophore degradation, as shown in Fig. 1. In addition, H_2O_2 enhances lignin solubility and reacts with the side-chain carbonyls and carbon-carbon double bonds, contributing to further oxidative degradation and improved lignin removal [41]. Organosolv extraction was employed as the initial delignification step because it relies solely on water and ethanol, which act synergistically to disrupt the bonds between cellulose and lignin [42]. Simultaneously, this process also solubilizes lignin macromolecules [5]. However, organosolv extraction alone does not sufficiently reduce the lignin content for nanocellulose production, as it typically leaves approximately 15 wt% of lignin in the substrate. Therefore, bleaching steps are commonly employed to further decrease lignin levels when needed.

3.2. Morphology of nanocelluloses

After delignification, the substrates underwent TEMPO oxidation using two NaClO concentrations (25 and 50 mmol/g substrate), followed by ultrasonication to produce nanocelluloses. Although these NaClO levels are higher than the typical range of 5–15 mmol/g [43], they were chosen to replicate a previous study on organosolv-bleached SCB, where such concentrations yielded CNC-like nanocelluloses [30]. In the present work, this experimental design was used to isolate the effect of delignification strategy, rather than oxidant dosage, on

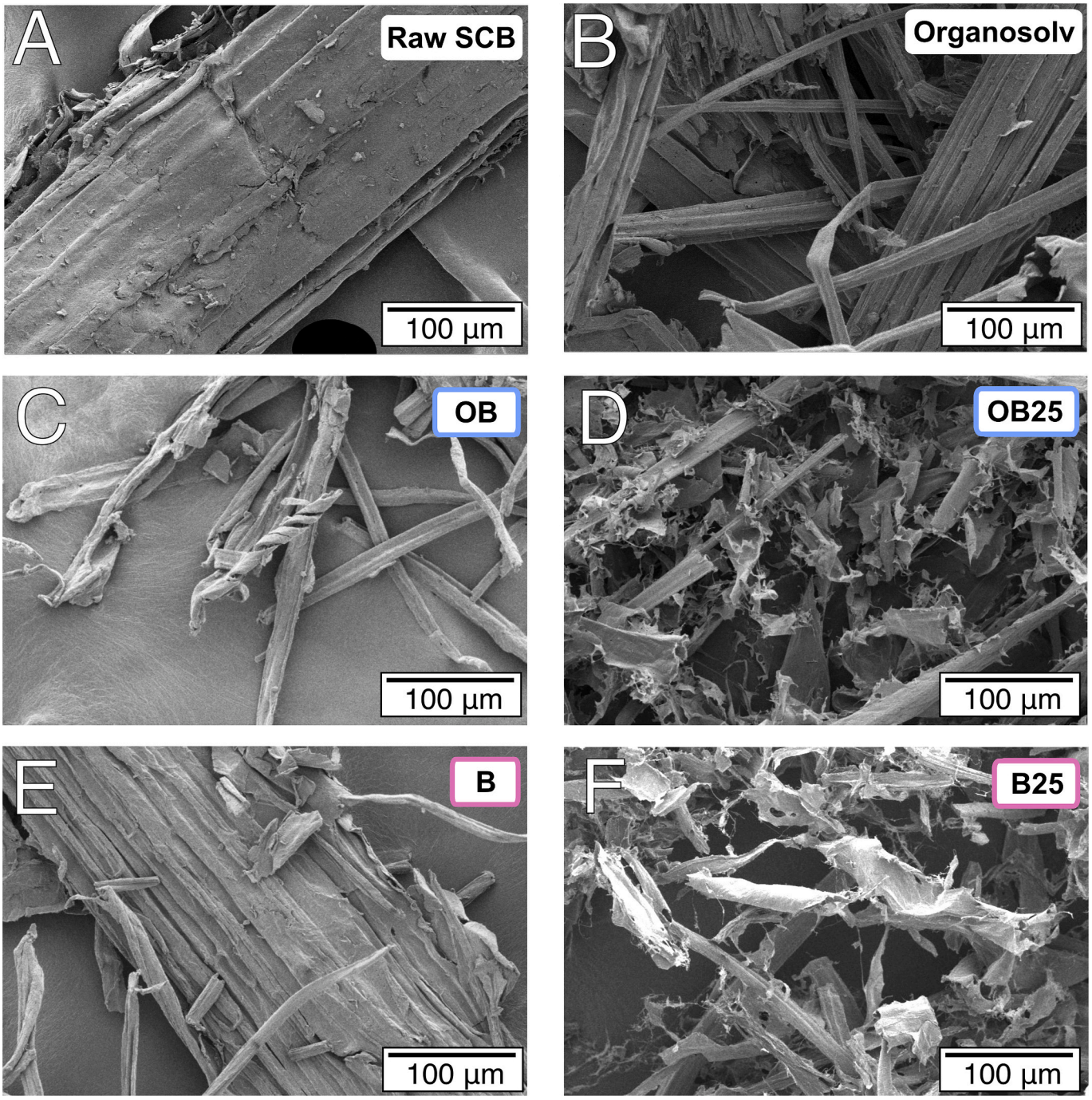

Fig. 3. FESEM images of raw SCB and substrates after delignification and oxidation: A) raw SCB, showing fiber bundles; B) Organosolv-treated SCB, with partially separated fibers; C-D) Organosolv-bleached substrates before (C) and after (D) TEMPO oxidation (25 mmol/g); E-F) Bleached-only SCB before (E) and after (F) TEMPO oxidation (25 mmol/g).

nanocellulose morphology. It also allowed us to explore whether a single bleaching could replace the two-step process used previously in the organosolv-bleached treatment.

Fig. 2 shows the morphology of prepared nanocelluloses. Regardless of the sample, the nanocellulose diameter remained within the 2–3 nm range. However, the length of the nanocelluloses was strongly influenced by the delignification strategy. Applying bleaching after organosolv extraction, rather than directly to SCB, significantly affected the final morphology, shifting the material classification between CNFs and CNCs.

A direct comparison between OB25US and B25US, which were prepared using the same oxidant dosage and mechanical treatment, revealed that the sequential organosolv-bleaching yielded in shorter particles, with average length of 190 nm (Fig. 2A), which fall within the CNC classification. On the other hand, the directly bleached substrate (B25US) produced longer nanocelluloses, with 343 nm length on average (Fig. 2B). Furthermore, length distribution analysis showed that OB25US particles were mostly shorter than 200 nm, while B25US displayed broader distribution, predominantly between 200 and 400. This distinction is particularly relevant given that both substrates exhibited similarly low lignin contents, suggesting that lignin content alone is not the primary determinant of nanocellulose morphology. In addition, sonicated OB25 and OB50 dispersions became highly fluid, even after only 5 min of probe ultrasonication, typical of CNC dispersions at this

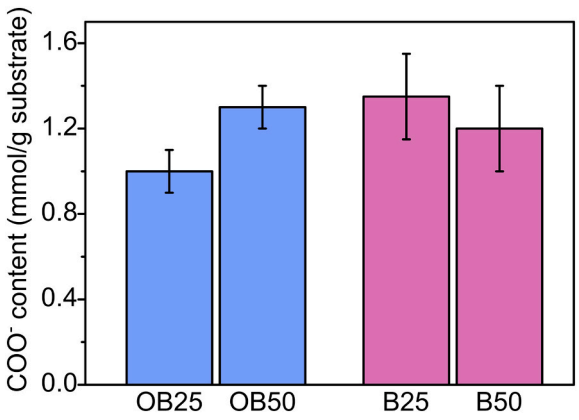

Fig. 4. Carboxylate content (COO^-) of TEMPO-oxidized samples, determined by conductometric titration. Values refer to sample oxidized with 25 or 50 mmol NaClO per gram of substrate.

concentration. Conversely, B25 and B50 dispersions became more viscous following ultrasonication, a behavior typical of CNF suspensions at this concentration, as discussed in detail below.

Similarly, when using 50 mmol NaClO/g substrate, the organosolv-bleached sample produced shorter particles (average length: 272 nm on average, Fig. 2C) compared to those from the directly bleached substrate (417 nm on average, Fig. 2D). This trend mirrors the results obtained with 25 mmol NaClO/g, confirming that the delignification strategy consistently influences nanocellulose morphology. However, for both substrates, the average nanocellulose length increased a little when the oxidant concentration was raised from 25 to 50 mmol/g.

After TEMPO oxidation, the remaining mass was similar across all samples: 81 ± 3 wt% for B25, 80 ± 4 wt% for B50, 80 ± 1 wt% for OB25, and 79 ± 2 wt% for OB50. The ~20 wt% mass loss is attributed to the formation of the water-soluble byproducts during oxidation [44]. The comparable post-oxidation yields across different NaClO concentrations suggest that the excess oxidant is likely consumed in over-oxidation of already accessible domains, rather than leading to increased yield losses.

The observed differences in nanocellulose morphology indicate that delignification plays a key role in determining particle length. Substrates subjected only to bleaching consistently produced longer fibrils, whereas those that underwent sequential organosolv-bleaching yielded shorter nanocelluloses. To clarify the mechanisms behind these morphological differences, the following sections explore the impact of delignification on fiber structure.

3.3. Effect of delignification history

Since the OB and B substrates presented similar overall chemical compositions (Table 1), with only slight differences, the observed differences in nanocellulose morphology cannot be attributed solely to composition. Instead, they are more plausibly explained by differences in fiber structure resulting from the delignification process. In particular, the greater fiber disruption promoted by sequential organosolv-bleaching enhanced fibril accessibility and separation both during TEMPO oxidation and mechanical treatment.

FESEM analysis (Fig. 3) reveals pronounced morphological differences in the bleached substrates obtained by the two routes. Untreated SCB (Fig. 3A) displays compact fibers composed mostly of cellulose, hemicellulose, and lignin [45]. Delignification via organosolv or bleaching exposes thinner fibers (Fig. 3B and E) since lignin acts as a binding agent, holding the fiber bundles together [46]. When bleaching is applied to a pre-delignified substrate, such as in the organosolv-treated samples, the substrate appears more fibrillated and disordered even before TEMPO-oxidation (Fig. 3C). The morphological disruption is attributed to the initial organosolv step, despite the substrate still retaining approximately 15 wt% lignin.

OB exhibited a lower hemicellulose content (13 wt%) than B (17 wt %) (Table 1). While hemicellulose can, in some cases, facilitate fibrillation by increasing fiber flexibility and reducing aggregation, in this case, the extent of fiber disruption in OB had a more pronounced effect, promoting easier fragmentation [47,48]. Likewise, lignin forms a network surrounding cellulose microfibrils, covalently linked to hemicelluloses through ester and ether bonds in lignin-carbohydrate complexes [49]. Hemicelluloses interact with cellulose surfaces via multiple hydrogen bonds, and with lignin through both covalent and non-covalent interactions, acting as a cohesive bridge between these two components [50]. This supramolecular arrangement maintains the integrity of the fiber bundles and limits the accessibility of reactants to cellulose microfibrils, which hinders their individualization. Therefore, the successive removal of lignin and hemicellulose during organosolv-bleaching leads to greater exposure of microfibrils and facilitates their fragmentation during TEMPO oxidation and mechanical treatment. This mechanistic insight explains why OB samples yielded shorter nanocelluloses (CNCs), in contrast to the CNFs from the B substrate. Notably, after TEMPO-oxidation, both OB25 and B25 samples appeared highly disaggregated, with micro- and nano-fibrillated regions already observable prior to any mechanical treatment (Fig. 3D and F, respectively).

The determination of cellulose DP revealed trends consistent with the morphological changes observed by SEM. Before TEMPO oxidation, the B sample showed a higher DP (647) than OB (533), indicating that the combination of organosolv extraction and bleaching promoted partial depolymerization of cellulose chains. After TEMPO oxidation, OB25 and B25 exhibited similar DPs (363 and 342, respectively), indicating that this step was a major contributor to chain depolymerization, as expected [51]. However, average DP alone does not capture differences in the supramolecular organization of cellulose chains. In this

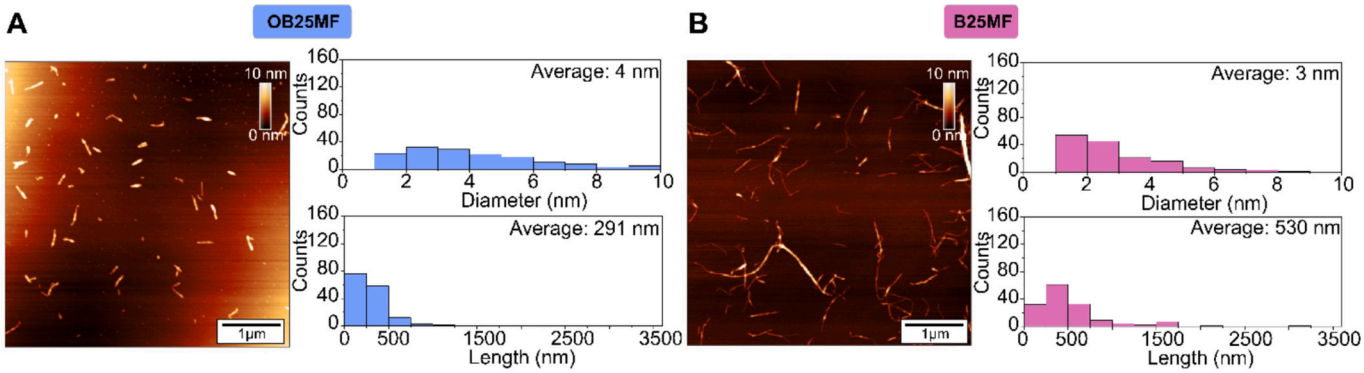

Fig. 5. AFM image and corresponding diameter and length distribution histograms of nanocelluloses obtained by microfluidization: A) OB25MF; and B) B25MF.

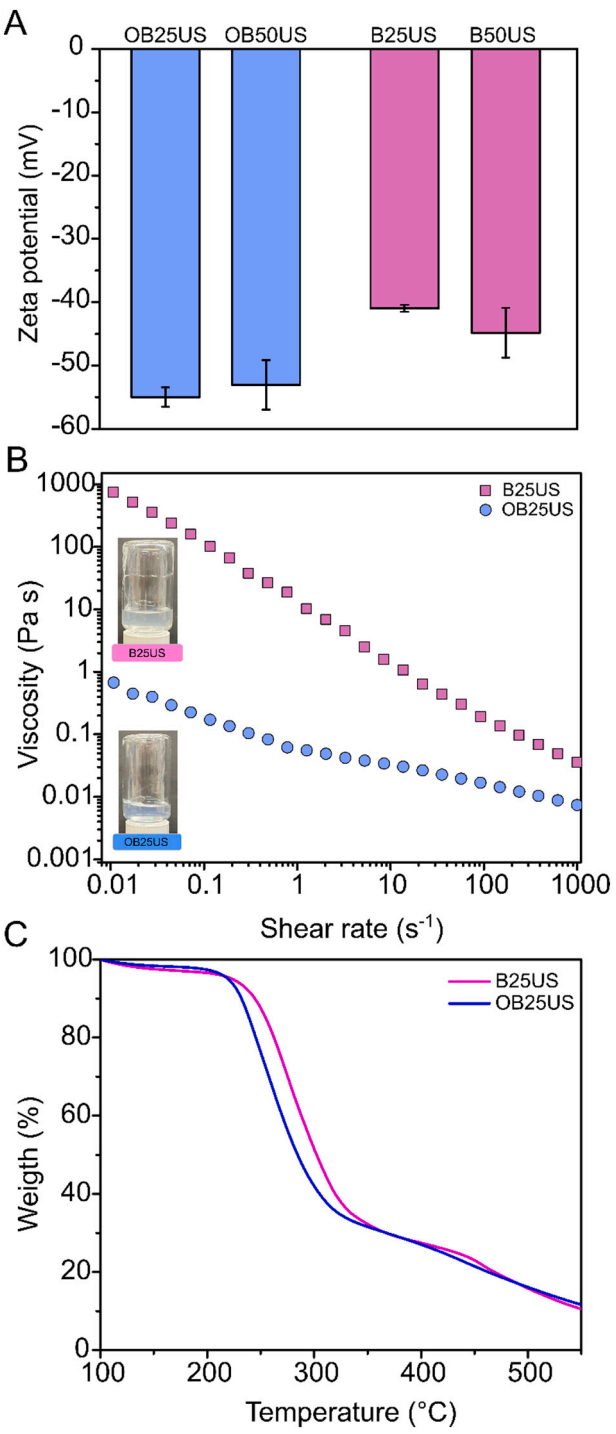

Fig. 6. Characterization of nanocelluloses: A) Zeta potential values of the prepared nanocelluloses, indicating their colloidal stability; B) flow curves from rheology measurements of aqueous nanocellulose suspensions at 1 wt%, along with representative images of the dispersions; and C) TGA curves showing the thermal degradation profiles.

context, OB substrates likely contain less cohesive fiber domains prior to TEMPO oxidation. Conversely, B substrates may have retained a more cohesive fibrillar network, leading to longer fibrils when fibrillated, despite reaching a similar DP after oxidation. This difference highlights the importance of processing history in explaining nanocellulose morphology and fragmentation behavior. Furthermore, viscosity-based DP reflects only average molecular weight and does not provide insight into the distribution. Thus, two samples with similar average DPs may differ substantially in polydispersity. This supports the notion that substrate morphology plays a critical role in fibrillation outcomes, including fiber damage, induced by delignification. In such cases, supramolecular interactions, such as fibril entanglement, can significantly influence mechanical disintegration, even if not evident in DP.

Fig. 4 presents the quantity of surface-oxidized groups (i.e., COO^-) on the substrates after TEMPO oxidation. The carboxylate contents ranged from 1.0 to 1.4 mmol/g substrate, consistent with previous values reported for SCB oxidized under comparable conditions [30]. A closer comparison between B and OB samples reveals some small differences in oxidation behaviors. When treated with 25 mmol NaClO/g, the B25 sample exhibited a higher carboxylate content (1.4 ± 0.2 mmol COO^-/g) than OB25 (1.0 ± 0.1 mmol/g). Interestingly, increasing NaClO concentration to 50 mmol/g resulted in a higher COO^- content for OB50 (1.3 ± 0.1 mmol/g), while B50 displayed a similar value to B25 (1.2 ± 0.2 mmol/g). This trend suggests that distinct oxidation dynamics between the two substrates, likely arising from differences during delignification. This difference is attributed to the fact that oxidation efficiency is influenced not only by chemical composition but also by fiber morphology, surface accessibility, and potential solubilization of cellulose fragments. The OB substrate, having undergone a more aggressive delignification, likely contained shorter chains and more disordered domains that were more susceptible to oxidation and solubilization during the reaction. As a result, part of the oxidizing agent may have been consumed in degrading soluble fragments, leading to lower COO^- content in the solid substrate.

The presence of carboxylate groups is a key factor for nanocellulose production, as these negatively charged groups enhance electrostatic repulsion between fibrils. This facilitates mechanical disintegration and helps stabilize the resulting dispersions by preventing aggregation [14].

3.4. Evaluation of microfluidization as an alternative mechanical treatment

In replacement to sonication, microfluidization was used as the mechanical treatment on selected samples to determine whether the observed differences in nanocellulose morphology were specifically related to the fibrillation method. In typical ultrasonication, fibrillation occurs through cavitation, a process in which microscopic bubbles are formed, expanded, and imploded, generating intense shear forces that break down the fiber structure [52,53]. Cavitation primarily affects the more fragile regions of the fibers, resulting in reductions in both diameter and length. On the other hand, the microfluidization forces the suspension through narrow interaction chambers under high pressure, applying shear and impact forces via a different mechanism [54].

Fig. 5 presents representative AFM images along with the diameter and length histograms of nanocelluloses produced via microfluidization. As observed previously with ultrasonication, OB yielded significantly shorter nanocelluloses compared to B, with average lengths of 291 nm and 530 nm, respectively. The difference indicates that the delignification strategy rather than the type of mechanical treatment, is the primary factor influencing nanocellulose morphology. It is important to highlight that microfluidization was performed under relatively mild conditions [20] to minimize excessive fiber damage and better isolate the effects of the delignification route on nanocellulose production.

3.5. Surface properties of nanocelluloses and rheology behavior of their suspensions

Fig. 6A shows zeta-potential values of the prepared nanocelluloses. The results indicate high colloidal stability, as the absolute values exceed 30 mV in modulus, which is a commonly accepted threshold for stable colloidal dispersions of nanocelluloses [55]. This behavior is attributed to the high content of surface carboxy groups introduced during TEMPO oxidation (Fig. 4). Nanocelluloses contained such functional groups exhibit strong hydrophilicity, making them suitable for

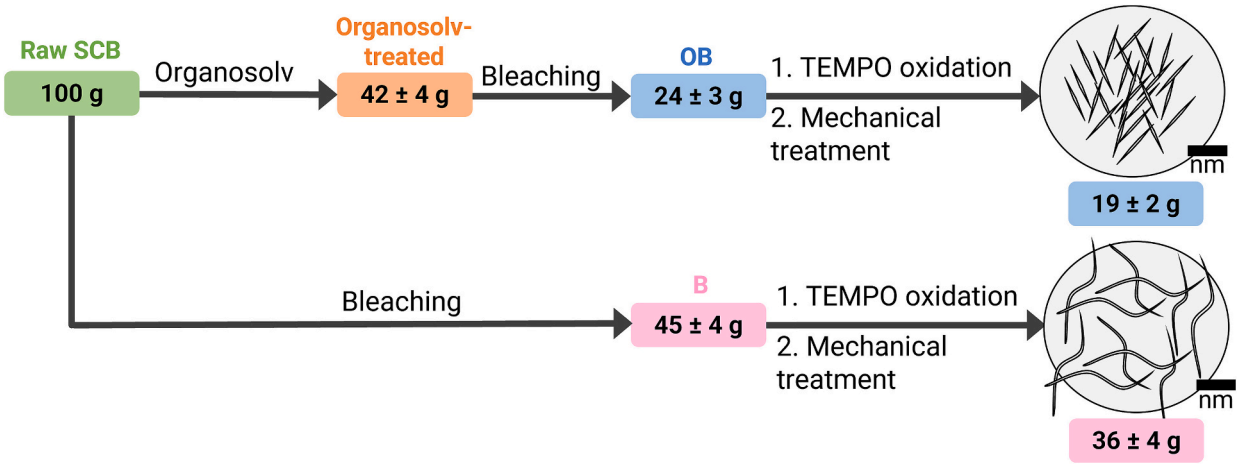

Fig. 7. Summary of the process yields for each step (delignification, TEMPO oxidation and fibrillation), comparing the two delignification strategies: sequential organosolv-bleaching and single-step bleaching.

applications in water-based systems such as films, gels, emulsions, and hydrogels [9,27].

Fig. 6B displays the flow curves of selected samples prepared at the concentration of 1 wt%. As expected, the dispersions exhibited shear-thinning behavior, which is typical of nanocellulose suspensions. This behavior is associated with the alignment and disentanglement of nanocelluloses under shear, reducing flow resistance and, consequently, viscosity [56]. The viscosity profiles varied considerably, correlating with the morphology of the nanocellulose produced. Sample B25US showed significant higher viscosities due to their strong ability to form entangled networks even at low concentrations, which is a behavior typical of CNFs [1]. Although these CNFs are shorter on average than those commonly obtained from wood pulp [57], they still exhibited high viscosities, likely due to the high surface charge and entanglement capacity [57]. On the other hand, short nanocelluloses such as those produced from OB25US (CNCs) do not readily form gels at this concentration. These particle suspensions displayed much lower viscosity values, as a higher concentration is typically required to promote sufficient interaction and network formation, which is similar to other CNC samples [25,58].

Finally, Fig. 6C presents the TGA curves for OB25US and B25US. Both nanocellulose samples showed an initial minor weight loss below 200 °C, attributed to the evaporation of adsorbed and bound water. Between 200 and 350 °C, thermal degradation occurred primarily due to the cellulose degradation [59]. T_{onset} for thermal degradation was 241 °C for B25US and 223 °C for OB25US. This difference is likely related to the more aggressive delignification steps used in preparing OB25US, which may have introduced additional chain ends that serves as initiation sites for earlier thermal degradation.

3.6. Process summary and considerations

Process yields should be interpreted in conjunction with nanocellulose characterization results. Fig. 7 summarizes the mass balance for both delignification strategies, taking 100 g of raw SCB as the initial input. The organosolv-bleached route yielded a lower amount of cellulose substrate (24 g) due to the two-step delignification process, which resulted in greater mass loss and ultimately led to a lower yield of nanocellulose (19 g). In fact, the organosolv extraction applied to raw SCB produced 42 g of pretreated material, which was subsequently bleached. In contrast, single-step bleaching applied directly to raw SCB produced 45 g of delignified substrate and yielded 36 g of CNFs. The reduction in nanocellulose yield relative to the delignified solids in both routes is primarily attributed to the ~20 wt% mass loss during TEMPO oxidation, which generates water-soluble byproducts [44].

The main differences between the resulting nanocelluloses lie in their morphology, which significantly affects their potential applications. B samples produced longer fibrils and formed more viscous suspensions, while OB samples yielded shorter fibrils with lower viscosity. Although the overall yield from the OB route was lower, it is important to note that the typical CNC yield obtained by H_2SO_4 hydrolysis is around 50 % of the cellulose content in the biomass under optimal conditions [60,61]. Therefore, the OB process offers a promising acid-free alternative for producing carboxylated CNCs [31].

From a biorefinery perspective, sequential organosolv-bleaching enables efficient recovery of lignin as a co-product with high value for materials and chemicals [5], which improves overall SCB valorization [62]. In contrast, lignin extracted from the single-bleaching method is less prone to recovery, as the oxidative treatment leads to extensive fragmentation, leaving most of it as acid-soluble oxidative byproducts. From a process standpoint, the B route offers operational advantages for CNF production by eliminating the organosolv step, reducing chemical and energy consumption, simplifying unit operations, and potentially lowering capital and operating costs. Considering the similar post-oxidation yields and performance for CNF, this route may be more preferable for large-scale applications, with the added possibility of using lower NaClO concentration for the single-step bleaching to produce CNFs. In contrast, the OB route is better suited for scenarios prioritizing product diversification, high-yield, and acid-free carboxylated CNCs, although it typically requires higher NaClO concentrations, as previously demonstrated [30]. This reflects a process-product trade-off, in which the optimal pathway depends on the desired product portfolio and specific market demands.

4. Conclusion

This study elucidated the impact of processing SCB substrates with similarly low lignin content but obtained through different delignification strategies on nanocellulose morphology. The findings demonstrated that morphology can be effectively tuned by modifying the delignification route alone, while keeping the oxidation conditions constant. Structural modifications induced by sequential organosolv-bleaching were essential for enabling the production of CNCs via TEMPO oxidation, while single-step bleaching favored the formation of CNFs. The comprehensive evaluation of chemical, surface, and morphological properties at each processing stage provides valuable insights into optimal pathways for preparing carboxylated CNFs via a single single-step route or carboxylated CNCs through an acid-free approach. These results broaden the design space for nanocellulose production and enable strategic selection of production routes tailored to specific

application requirements.

CRediT authorship contribution statement

Eupidio Scopel: Writing – review & editing, Writing – original draft, Validation, Methodology, Investigation, Formal analysis, Data curation, Conceptualization. **Lidiane O. Pinto:** Writing – original draft, Methodology, Investigation, Data curation. **Camila A. Rezende:** Writing – review & editing, Writing – original draft, Validation, Supervision, Resources, Project administration, Methodology, Investigation, Funding acquisition, Formal analysis, Conceptualization.

Declaration of Generative AI and AI-assisted technologies in the writing process

During the preparation of this work the authors used ChatGPT in order to improve language and readability. After using this tool/service, the authors reviewed and edited the content as needed and take full responsibility for the content of the publication.

Funding

This work was supported by São Paulo Research Foundation (grants number 15/13684-0, 19/19360-3, 21/12071-6, 23/01620-4); Conselho Nacional de Desenvolvimento Científico e Tecnológico (142570/2019-2), and financed in part by the Coordenação de Aperfeiçoamento de Pessoal de Nível Superior - Brasil (CAPES) - Finance Code 001.

Declaration of competing interest

The authors declare that they have no known competing financial interests or personal relationships that could have appeared to influence the work reported in this paper.

Acknowledgements

The authors thank Dr. Fernando Galembeck for AFM access; Dr. Juliana Bernardes and the Brazilian Nanotechnology National Laboratory (LNNano/CNPEM) for microfluidizer access; and Dr. Edvaldo Sabadini and Fernando Bonin Okasaki for rheology measurements. We thank the LIMicro-IQ – Microscopy Core Facility (RRID:SCR_024633) at the Universidade Estadual de Campinas for support. The Quanta FEG 250 system was partially funded by a FAPESP grant #23/01620-4 for the LIMicro-IQ Core Facility.

Data availability

Data will be made available on request.

References

[1] K.J. De France, T. Hoare, E.D. Cranston, Review of hydrogels and aerogels containing nanocellulose, Chem. Mater. 29 (2017) 4609–4631, https://doi.org/10.1021/acs.chemmater.7b00531.
[2] R.J. Moon, A. Martini, J. Nairn, J. Simonsen, J. Youngblood, Cellulose nanomaterials review: structure, properties and nanocomposites, Chem. Soc. Rev. 40 (2011) 3941–3994, https://doi.org/10.1039/C0CS00108B.
[3] M. Mujtaba, L. Fernandes Fraceto, M. Fazeli, S. Mukherjee, S.M. Savassa, G. Araujo de Medeiros, A. do Espírito Santo Pereira, S.D. Mancini, J. Lipponen, F. Vilaplana, Lignocellulosic biomass from agricultural waste to the circular economy: a review with focus on biofuels, biocomposites and bioplastics, J. Clean. Prod. 402 (2023) 136815, https://doi.org/10.1016/j.jclepro.2023.136815.
[4] P. Yadav, S. Kumar Anu, V. Tiwari, D. Kumar, S. Kumar Singh, V. Manisha, B. Singh Malik, Sugarcane bagasse: an important lignocellulosic substrate for production of enzymes and biofuels, Biomass Convers. Biorefinery 14 (2024) 6111–6142, https://doi.org/10.1007/s13399-022-02791-9.
[5] S.C. Rabelo, P.Y.S. Nakasu, E. Scopel, M.F. Araújo, L.H. Cardoso, A.C. da Costa, Organosolv pretreatment for biorefineries: current status, perspectives, and challenges, Bioresour. Technol. (2022) 128331, https://doi.org/10.1016/j.biortech.2022.128331.
[6] O. Rosales-Calderon, V. Arantes, A review on commercial-scale high-value products that can be produced alongside cellulosic ethanol, Biotechnol. Biofuels 12 (2019) 240, https://doi.org/10.1186/s13068-019-1529-1.
[7] H. Du, W. Liu, M. Zhang, C. Si, X. Zhang, B. Li, Cellulose nanocrystals and cellulose nanofibrils based hydrogels for biomedical applications, Carbohydr. Polym. 209 (2019) 130–144, https://doi.org/10.1016/j.carbpol.2019.01.020.
[8] F. Hoeng, A. Denneulin, J. Bras, Use of nanocellulose in printed electronics: a review, Nanoscale 8 (2016) 13131–13154, https://doi.org/10.1039/C6NR03054H.
[9] S.J. Eichhorn, A. Dufresne, M. Aranguren, N.E. Marcovich, J.R. Capadona, S. J. Rowan, C. Weder, W. Thielemans, M. Roman, S. Renneckar, W. Gindl, S. Veigel, J. Keckes, H. Yano, K. Abe, M. Nogi, A.N. Nakagaito, A. Mangalam, J. Simonsen, A. S. Benight, A. Bismarck, L.A. Berglund, T. Peijs, Review: current international research into cellulose nanofibres and nanocomposites, J. Mater. Sci. 45 (2010) 1–33, https://doi.org/10.1007/s10853-009-3874-0.
[10] E.S. Ferreira, C.A. Rezende, E.D. Cranston, Fundamentals of cellulose lightweight materials: bio-based assemblies with tailored properties, Green Chem. 23 (2021) 3542–3568, https://doi.org/10.1039/D1GC00326G.
[11] Z. Fang, G. Hou, C. Chen, L. Hu, Nanocellulose-based films and their emerging applications, Curr. Opin. Solid State Mater. Sci. 23 (2019) 100764, https://doi.org/10.1016/j.cossms.2019.07.003.
[12] S.A. Kedzior, V.A. Gabriel, M.A. Dubé, E.D. Cranston, Nanocellulose in emulsions and heterogeneous water-based polymer systems: a review, Adv. Mater. 33 (2021) 2002404, https://doi.org/10.1002/adma.202002404.
[13] T. Abitbol, A. Rivkin, Y. Cao, Y. Nevo, E. Abraham, T. Ben-Shalom, S. Lapidot, O. Shoseyov, Nanocellulose, a tiny fiber with huge applications, Curr. Opin. Biotechnol. 39 (2016) 76–88, https://doi.org/10.1016/j.copbio.2016.01.002.
[14] A. Isogai, T. Saito, H. Fukuzumi, TEMPO-oxidized cellulose nanofibers, Nanoscale 3 (2011) 71–85, https://doi.org/10.1039/C0NR00583E.
[15] H. Dong, J.F. Snyder, K.S. Williams, J.W. Andzelm, Cation-induced hydrogels of cellulose nanofibrils with tunable moduli, Biomacromolecules 14 (2013) 3338–3345, https://doi.org/10.1021/bm400993f.
[16] B. Frka-Petesic, T.G. Parton, C. Honorato-Rios, A. Narkevicius, K. Ballu, Q. Shen, Z. Lu, Y. Ogawa, J.S. Haataja, B.E. Droguet, R.M. Parker, S. Vignolini, Structural color from cellulose nanocrystals or chitin nanocrystals: self-assembly, optics, and applications, Chem. Rev. 123 (2023) 12595–12756, https://doi.org/10.1021/acs.chemrev.2c00836.
[17] D. Trache, A.F. Tarchoun, M. Derradji, T.S. Hamidon, N. Masruchin, N. Brosse, M. H. Hussin, Nanocellulose: from fundamentals to advanced applications, Front. Chem. 8 (2020). https://www.frontiersin.org/articles/10.3389/fchem.2020.00392. (Accessed 9 November 2023).
[18] T. Saito, M. Hirota, N. Tamura, S. Kimura, H. Fukuzumi, L. Heux, A. Isogai, Individualization of nano-sized plant cellulose fibrils by direct surface carboxylation using TEMPO catalyst under neutral conditions, Biomacromolecules 10 (2009) 1992–1996, https://doi.org/10.1021/bm900414t.
[19] P. Bajpai, P. Bajpai, Chapter 4 - production of nanocellulose, in: Pulp Pap. Ind., Elsevier, 2017, pp. 41–67, https://doi.org/10.1016/B978-0-12-811101-7.00004-6.
[20] C. Carneiro Pessan, J. Silva Bernardes, S.H.P. Bettini, E.R. Leite, Oxidized cellulose nanofibers from sugarcane bagasse obtained by microfluidization: Morphology and rheological behavior, Carbohydr. Polym. 304 (2023) 120505, https://doi.org/10.1016/j.carbpol.2022.120505.
[21] T. Saito, S. Kimura, Y. Nishiyama, A. Isogai, Cellulose nanofibers prepared by TEMPO-mediated oxidation of native cellulose, Biomacromolecules 8 (2007) 2485–2491, https://doi.org/10.1021/bm0703970.
[22] F. Rol, S. Saini, V. Meyer, M. Petit-Conil, J. Bras, Production of cationic nanofibrils of cellulose by twin-screw extrusion, Ind. Crop. Prod. 137 (2019) 81–88, https://doi.org/10.1016/j.indcrop.2019.04.031.
[23] V. Arantes, I.K.R. Dias, G.L. Berto, B. Pereira, B.S. Marotti, C.F.O. Nogueira, The current status of the enzyme-mediated isolation and functionalization of nanocelluloses: production, properties, techno-economics, and opportunities, Cellulose 27 (2020) 10571–10630, https://doi.org/10.1007/s10570-020-03332-1.
[24] B.R. Rossi, V.O.A. Pellegrini, A.A. Cortez, E.M.S. Chiromito, A.J.F. Carvalho, L. O. Pinto, C.A. Rezende, V.R. Mastelaro, I. Polikarpov, Cellulose nanofibers production using a set of recombinant enzymes, Carbohydr. Polym. 256 (2021) 117510, https://doi.org/10.1016/j.carbpol.2020.117510.
[25] G. Delepierre, O.M. Vanderfleet, E. Niinivaara, B. Zakani, E.D. Cranston, Benchmarking cellulose nanocrystals part II: new industrially produced materials, Langmuir 37 (2021) 8393–8409, https://doi.org/10.1021/acs.langmuir.1c00550.
[26] M.S. Reid, M. Villalobos, E.D. Cranston, Benchmarking cellulose nanocrystals: from the laboratory to industrial production, Langmuir 33 (2017) 1583–1598, https://doi.org/10.1021/acs.langmuir.6b03765.
[27] Y. Habibi, L.A. Lucia, O.J. Rojas, Cellulose nanocrystals: chemistry, self-assembly, and applications, Chem. Rev. 110 (2010) 3479–3500, https://doi.org/10.1021/cr900339w.
[28] O.M. Vanderfleet, E.D. Cranston, Production routes to tailor the performance of cellulose nanocrystals, Nat. Rev. Mater. 6 (2021) 124–144, https://doi.org/10.1038/s41578-020-00239-y.
[29] C.H.M. Camargos, C.A. Rezende, Structure–property relationships of cellulose nanocrystals and nanofibrils: implications for the design and performance of nanocomposites and all-nanocellulose systems, ACS Appl. Nano Mater. 4 (2021) 10505–10518, https://doi.org/10.1021/acsanm.1c02008.
[30] L.O. Pinto, J.S. Bernardes, C.A. Rezende, Low-energy preparation of cellulose nanofibers from sugarcane bagasse by modulating the surface charge density, Carbohydr. Polym. 218 (2019) 145–153, https://doi.org/10.1016/j.carbpol.2019.04.070.

[31] Y. Zhou, T. Saito, L. Bergström, A. Isogai, Acid-free preparation of cellulose nanocrystals by TEMPO oxidation and subsequent cavitation, Biomacromolecules 19 (2018) 633–639, https://doi.org/10.1021/acs.biomac.7b01730.
[32] A.S. da Silva, H. Inoue, T. Endo, S. Yano, E.P.S. Bon, Milling pretreatment of sugarcane bagasse and straw for enzymatic hydrolysis and ethanol fermentation, Bioresour. Technol. 101 (2010) 7402–7409, https://doi.org/10.1016/j.biortech.2010.05.008.
[33] A.O. Kane, E. Scopel, A.A. Cortez, B.R. Rossi, V.O.A. Pellegrini, C.A. Rezende, I. Polikarpov, Enzyme-assisted production of cellulose nanofibers from bleached and bleached/sulfonated sugarcane bagasse: impact of sulfonation on nanocellulose properties and yields, Cellulose 30 (2023) 11507–11520, https://doi.org/10.1007/s10570-023-05600-2.
[34] A. Sluiter, B. Hames, R. Ruiz, C. Scarlata, J. Sluiter, D. Templeton, D. Crocker, Determination of Structural Carbohydrates and Lignin in Biomass, Technical Report NREL/TP-510-42618, National Renewable ENergy Laboratory, Golden, CO, USA, 2008.
[35] M. Henriksson, L.A. Berglund, P. Isaksson, T. Lindström, T. Nishino, Cellulose nanopaper structures of high toughness, Biomacromolecules 9 (2008) 1579–1585, https://doi.org/10.1021/bm800038n.
[36] M. Marx-Figini, Significance of the intrinsic viscosity ratio of unsubstituted and nitrated cellulose in different solvents, Angew. Makromol. Chem. 72 (1978) 161–171, https://doi.org/10.1002/apmc.1978.050720114.
[37] S. Katz, R.P. Beatson, M.S. Anthony, The determination of strong and weak acidic groups in sulfite pulps, in: Svensk Papperstidning-Nordisk Celulosa 87, 1984, pp. 48–53.
[38] S.C. Rabelo, L.B. Brenelli, T.C. Pin, E. Scopel, A.C. da Costa, Chapter 5 - pretreatments as a key for enzymatic hydrolysis of lignocellulosic biomass, in: R. Goldbeck, P. Poletto (Eds.), Polysacch.-Degrading Biocatal, Academic Press, 2023, pp. 109–137, https://doi.org/10.1016/B978-0-323-99986-1.00003-X.
[39] F.B. de Oliveira, J. Bras, M.T. Borges Pimenta, A.A. da Silva Curvelo, M. N. Belgacem, Production of cellulose nanocrystals from sugarcane bagasse fibers and pith, Ind. Crop. Prod. 93 (2016) 48–57, https://doi.org/10.1016/j.indcrop.2016.04.064.
[40] G. Banerjee, S. Car, J.S. Scott-Craig, D.B. Hodge, J.D. Walton, Alkaline peroxide pretreatment of corn stover: effects of biomass, peroxide, and enzyme loading and composition on yields of glucose and xylose, Biotechnol. Biofuels 4 (2011) 16, https://doi.org/10.1186/1754-6834-4-16.
[41] G. Wu, M. Heitz, E. Chornet, The depolymerization of lignin via aqueous alkaline oxidation, in: A.V. Bridgwater (Ed.), Adv. Thermochem. Biomass Convers., Springer Netherlands, Dordrecht, 1993, pp. 1558–1571, https://doi.org/10.1007/978-94-011-1336-6_127.
[42] L.G. Nair, K. Agrawal, P. Verma, Organosolv pretreatment: an in-depth purview of mechanics of the system, Bioresour. Bioprocess. 10 (2023) 50, https://doi.org/10.1186/s40643-023-00673-0.
[43] H. Xu, J.L. Sanchez-Salvador, A. Balea, A. Blanco, C. Negro, Optimization of reagent consumption in TEMPO-mediated oxidation of Eucalyptus cellulose to obtain cellulose nanofibers, Cellulose 29 (2022) 6611–6627, https://doi.org/10.1007/s10570-022-04672-w.
[44] A. Tejado, Md.N. Alam, M. Antal, H. Yang, T.G.M. van de Ven, Energy requirements for the disintegration of cellulose fibers into cellulose nanofibers, Cellulose 19 (2012) 831–842, https://doi.org/10.1007/s10570-012-9694-4.
[45] C.A. Rezende, M.A. de Lima, P. Maziero, E.R. deAzevedo, W. Garcia, I. Polikarpov, Chemical and morphological characterization of sugarcane bagasse submitted to a delignification process for enhanced enzymatic digestibility, Biotechnol. Biofuels 4 (2011) 54, https://doi.org/10.1186/1754-6834-4-54.
[46] B. Monties, Plant cell walls as fibrous lignocellulosic composites: relations with lignin structure and function, Anim. Feed Sci. Technol. 32 (1991) 159–175, https://doi.org/10.1016/0377-8401(91)90019-O.
[47] S. Arola, J.-M. Malho, P. Laaksonen, M. Lille, M.B. Linder, The role of hemicellulose in nanofibrillated cellulose networks, Soft Matter 9 (2012) 1319–1326, https://doi.org/10.1039/C2SM26932E.
[48] A. Khodayari, W. Thielemans, U. Hirn, A.W. Van Vuure, D. Seveno, Cellulose-hemicellulose interactions — a nanoscale view, Carbohydr. Polym. 270 (2021) 118364, https://doi.org/10.1016/j.carbpol.2021.118364.
[49] D. Tarasov, M. Leitch, P. Fatehi, Lignin–carbohydrate complexes: properties, applications, analyses, and methods of extraction: a review, Biotechnol. Biofuels 11 (2018) 269, https://doi.org/10.1186/s13068-018-1262-1.
[50] O.M. Terrett, P. Dupree, Covalent interactions between lignin and hemicelluloses in plant secondary cell walls, Curr. Opin. Biotechnol. 56 (2019) 97–104, https://doi.org/10.1016/j.copbio.2018.10.010.
[51] T. Saito, A. Isogai, TEMPO-mediated oxidation of native cellulose. The effect of oxidation conditions on chemical and crystal structures of the water-insoluble fractions, Biomacromolecules 5 (2004) 1983–1989, https://doi.org/10.1021/bm0497769.
[52] S.S. Hassan, G.A. Williams, A.K. Jaiswal, Emerging technologies for the pretreatment of lignocellulosic biomass, Bioresour. Technol. 262 (2018) 310–318, https://doi.org/10.1016/j.biortech.2018.04.099.
[53] D.Y. Hoo, Z.L. Low, D.Y.S. Low, S.Y. Tang, S. Manickam, K.W. Tan, Z.H. Ban, Ultrasonic cavitation: an effective cleaner and greener intensification technology in the extraction and surface modification of nanocellulose, Ultrason. Sonochem. 90 (2022) 106176, https://doi.org/10.1016/j.ultsonch.2022.106176.
[54] A. Khan, K.D. Vu, G. Chauve, J. Bouchard, B. Riedl, M. Lacroix, Optimization of microfluidization for the homogeneous distribution of cellulose nanocrystals (CNCs) in biopolymeric matrix, Cellulose 21 (2014) 3457–3468, https://doi.org/10.1007/s10570-014-0361-9.
[55] E. Johan Foster, R.J. Moon, U.P. Agarwal, M.J. Bortner, J. Bras, S. Camarero-Espinosa, K.J. Chan, M.J.D. Clift, E.D. Cranston, S.J. Eichhorn, D.M. Fox, W. Y. Hamad, L. Heux, B. Jean, M. Korey, W. Nieh, K.J. Ong, M.S. Reid, S. Renneckar, R. Roberts, J. Anne Shatkin, J. Simonsen, K. Stinson-Bagby, N. Wanasekara, J. Youngblood, Current characterization methods for cellulose nanomaterials, Chem. Soc. Rev. 47 (2018) 2609–2679, https://doi.org/10.1039/C6CS00895J.
[56] T. Moberg, K. Sahlin, K. Yao, S. Geng, G. Westman, Q. Zhou, K. Oksman, M. Rigdahl, Rheological properties of nanocellulose suspensions: effects of fibril/particle dimensions and surface characteristics, Cellulose 24 (2017) 2499–2510, https://doi.org/10.1007/s10570-017-1283-0.
[57] L. Jowkarderis, T.G.M. van de Ven, Rheology of semi-dilute suspensions of carboxylated cellulose nanofibrils, Carbohydr. Polym. 123 (2015) 416–423, https://doi.org/10.1016/j.carbpol.2015.01.067.
[58] M. Chau, S.E. Sriskandha, D. Pichugin, H. Thérien-Aubin, D. Nykypanchuk, G. Chauve, M. Méthot, J. Bouchard, O. Gang, E. Kumacheva, Ion-mediated gelation of aqueous suspensions of cellulose nanocrystals, Biomacromolecules 16 (2015) 2455–2462, https://doi.org/10.1021/acs.biomac.5b00701.
[59] H. Fukuzumi, T. Saito, Y. Okita, A. Isogai, Thermal stabilization of TEMPO-oxidized cellulose, Polym. Degrad. Stab. 95 (2010) 1502–1508, https://doi.org/10.1016/j.polymdegradstab. 2010.06.015.
[60] S.A. Nascimento, C.A. Rezende, Combined approaches to obtain cellulose nanocrystals, nanofibrils and fermentable sugars from elephant grass, Carbohydr. Polym. 180 (2018) 38–45, https://doi.org/10.1016/j.carbpol.2017.09.099.
[61] F.T. Seta, X. An, L. Liu, H. Zhang, J. Yang, W. Zhang, S. Nie, S. Yao, H. Cao, Q. Xu, Y. Bu, H. Liu, Preparation and characterization of high yield cellulose nanocrystals (CNC) derived from ball mill pretreatment and maleic acid hydrolysis, Carbohydr. Polym. 234 (2020) 115942, https://doi.org/10.1016/j.carbpol.2020.115942.
[62] E. Scopel, C.H.M. Camargos, L.O. Pinto, H. Trevisan, E.S. Ferreira, C.A. Rezende, Broadening the product portfolio with cellulose and lignin nanoparticles in an elephant grass biorefinery, Biofuels Bioprod. Biorefin. 17 (2023) 859–872, https://doi.org/10.1002/bbb.2476.